Muonic X-ray spectroscopy at MuSIC to measure nuclear sizes

T. Y. Saito[1,2], M. Niikura[2], T. Matsuzaki[3], H. Sakurai[2,3], M. Igashira[4], H. Imao[3], K. Ishida[3], T. Katabuchi[4], Y. Kawashima[5], M. K. Kubo[6], Y. Miyake[1], Y. Mori[7], K. Ninomiya[8,9], A. Sato[8,5], K. Shimomura[1], P. Strasser[1], A. Taniguchi[7], D. Tomono[5], and Y. Watanabe[3]

[1] *Graduate School of Science, the University of Tokyo, 7-3-1 Hongo, Bunkyo-ku, 113-0033 Tokyo, Japan*

[2] *Institute of Materials Structure Science, High Energy Accelerator Research Organization, 1-1 Oho, Tsukuba-shi, 305-0801 Ibaraki, Japan*

[3] *RIKEN Nishina Center, RIKEN, 2-1 Hirosawa, Wako-shi, 351-0198 Saitama, Japan*

[4] *Laboratory for Advanced Nuclear Energy, Institute of Science Tokyo, 2-12-1 Ookayama, Meguro-ku, 152-8550 Tokyo, Japan*

[5] *Research Center for Nuclear Physics, the University of Osaka, 10-1 Mihogaoka, Ibaraki-shi, 567-0047 Osaka, Japan*

[6] *Graduate School of Science, International Christian University, 3-10-2 Osawa, Mitaka-shi, 181-0015 Tokyo, Japan*

[7] *Institute for Integrated Radiation and Nuclear Science, Kyoto University, 2 Asashiro-Nishi, Kumatori-cho, Sennan-gun, 590-0494 Osaka, Japan*

[8] *Graduate School of Science, the University of Osaka, 1-1 Machikaneyama-cho, Toyonaka-shi, 560-0043 Osaka, Japan*

[9] *Natural Science Center for Basic Research and Development, Hiroshima University, 1-3-2 Kagamiyama, Higashi-Hiroshima-shi, 739-8511 Hiroshima, Japan*

1 Introduction

The nuclear charge radius is one of the most fundamental parameters for characterizing an atomic nucleus as a finite quantum many-body system. The muonic X-ray spectroscopy, namely characteristic X-ray spectroscopy of a muonic atom, is the most commonly used method to determine the absolute nuclear charge radius along with the electron scattering cross section measurement. These two methods have mostly the same accuracy for the radii and are complementary in terms of the experimental uncertainty [2, 3].

In this study [1], we measured the muonic X-ray transition energies of five palladium isotopes with the mass numbers $A = 104, 105, 106, 108$, and 110 to re-evaluate their nuclear charge radius. Although the $2p$-$1s$ transition energies are summarized in the table of ref. [2], the original paper is not published. In addition to the $2p$-$1s$ transitions, we experimentally determine higher transition energies including $3d$-$2p$ and $4f$-$3d$. These higher transitions play an important role in restricting the degrees of freedom in the parameter space of the nuclear charge distribution, as we discuss later in this article.

2 Experiment

The experiment was performed at the MuSIC-M1 beamline at Research Center for Nuclear Physics (RCNP). The muon beam momentum was chosen to be 50 MeV/c and decelerated to 40 MeV/c by a graphite degrader to maximize the muon stopped in the target. Isotopically-enriched palladium targets, with the mass number $A = 104$, 105, 106, 108, and 110, were used in order to separate neighboring X-ray lines diverged by the isotope shift. The target shapes were metal discs or metal powder, whose effective thickness against the beam was approximately 1 mm each.

Three plastic-scintillator-based beamline detectors were used to determine the muon beam event. Two detectors which were placed upstream of the target define the muon beam arrival time and also discriminate the contaminant electrons from the muon beam. The other detector was placed downstream side, and used as a VETO counter, which ensured the beam muon stopped in the target. Four high-purity germanium semiconductor detectors (HPGe) were used to measure the muonic X-rays. The pulse height of the the HPGe signals were recorded with a conventional peak-holding Analog-to-Digital Converter(ADC) after spectroscopic amplifiers.

3 Result and discussion

3.1 Muonic X-ray spectra

The photon energy spectrum measured with the ^{108}Pd target is shown in Figure 1. The beam-coincident events are selected using the time difference between the photon arrival time at the HPGe detectors and the muon

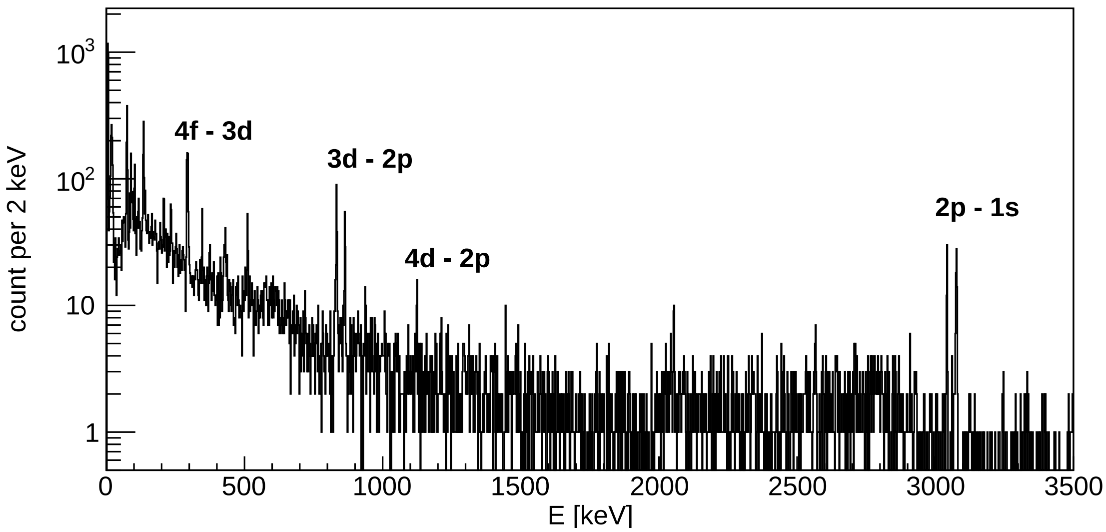

Figure 1: The photon spectrum measured with the ^{108}Pd target. The intense peaks are indicated. Figure is quoted from [1] (the same hereafter).

stop time determined by the beamline detectors. Each X-ray peak is fitted with a gaussian function considering the detector resolution and a constant background term. The mean energies of each transition are summarized in Table III and IV in [1].

It is worth to be noted that the muon-induced γ rays were also observed in the experiment. Those γ rays were emitted following the nuclear muon capture reaction, and have a time structure that decays along with the lifetime of the muonic atom. We have also determined the lifetime of each muonic palladium atom and discussed its isotope dependence in [1] although it is out of scope of this article.

3.2 theoretical interpretation

One must tackle the inverse problem to deduce nuclear charge radii from muonic X-ray energy. In other words, the charge distribution that consistently reproduces the experimental X-ray energy(s) needs to be determined numerically to deduce the charge radius.

We calculated the binding energy of the muonic atom with the Dirac equation describing a simple two-body bound system of the muon and nucleus. Statistic electric interaction

$$H_{\mu-N} = -\alpha \int \frac{\rho(r)}{|r-r'|} \mathrm{d}r' \tag{1}$$

was considered, where α is the fine structure constant and $\rho(r)$ is the nuclear charge dencity distribution. Two parameter Fermi function

$$\rho_{2\mathrm{pF}}(r) = \frac{N_0}{1+\exp\left[\frac{(r-c)}{t/(4\ln 3)}\right]} \tag{2}$$

was used to parametrize the nuclear charge density (normalized as $\int \rho \mathrm{d}r = Z$). c is the half-density radius and t corresponds to the surface diffuseness. After solving the Dirac equation, the first order QED correction, relativistic recoil correction, electron screening correction, and nuclear polarization correction were considered. See the original paper[1] or its references [4, 5, 6] for the detail of the calculation.

Once the muonic X-ray energies are obtained, one can compare them with the experimental data. The (assumed) charge distribution leads the list of X-ray energies; the charge distribution that we must obtain needs to be consistent with all of the measured X-ray transitions. We searched the parameter pair (c,t) that fulfill this condition with χ^2 minimization procedure. Figure 2 illustrates the 1σ consistent region in the parameter space of c-t for ^{108}Pd. Table 1 summarizes the determined charge distribution parameters and root-mean-square (rms) radii for each even isotope.

In that strategy, using multiple series of muonic transition is essential. The slope of two $3d$-$2p$ transitions are different from that of $2p$-$1s$ in Fig. 2, which enables us to determine two parameters. The χ^2 minimization principle provides not only the parameters themselves, but also the parameter uncertainties. Adding more

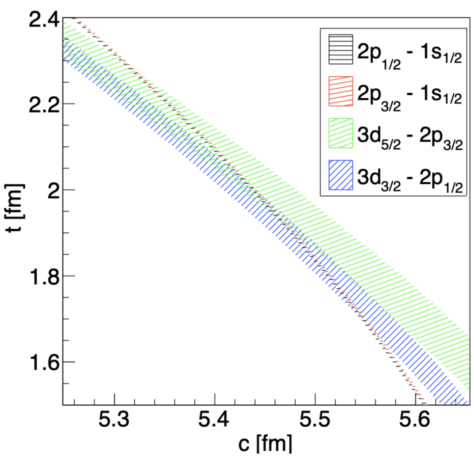

Figure 2: 1σ region limited by the obtained muonic transition energies in the two-dimensional c-t space for ^{108}Pd. Each shaded area corresponds to limited region by each muonic transition with 1σ uncertainty

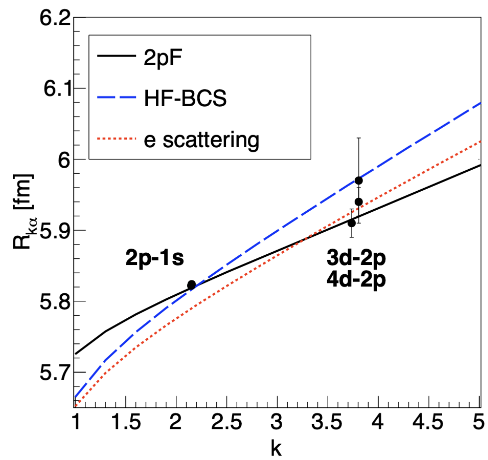

Figure 3: Barrett equivalent radii for each index k for ^{108}Pd. Five transitions of $2p$-$1s$, $3d$-$2p$, and $4d$-$2p$ are plotted as black dot. Note that two transitions of $2p$-$1s$ are overlapped each other. The dotted lines are calculated from the nuclear charge distribution obtained in previous works: the theoretical calculation based on Hartree-Fock BCS [10, 11, 12] and electron scattering experiment [13].

Table 1: Determined charge distribution parameters and rms radii for even palladium isotopes. The experimental uncertainties are also given.

	c (fm])	t (fm)	rms radius (fm)
^{104}Pd	5.26(12)	2.25(25)	4.493^{+28}_{-7}
^{106}Pd	5.49(30)	1.76(65)	4.507^{+96}_{-5}
^{108}Pd	5.45(11)	1.96(27)	4.537^{+27}_{-6}
^{110}Pd	5.60(26)	1.61(70)	4.548^{+100}_{-6}

independent transition lines limits the permitted area in the parameter space, and thus helps to reduce the uncertainty of the parameters. Therefore, adopting higher muonic transitions, such as $3d$-$2p$, in addition to $2p$-$1s$ are important to discuss nuclear charge radius.

One can visualize how each muonic transition restricts possible nuclear charge distribution by another theoretical approach. Barrett indicated that each muonic transition energy corresponds to a certain *nuclear moment* [7, 8, 9]:

$$\langle r^k e^{-\alpha_B r}\rangle = \frac{1}{Z}\int \rho(r) r^k e^{-\alpha_B r} 4\pi r^2 \mathrm{d}r. \tag{3}$$

Note that the index k can be non-integer. α_B is a parameter, which can be assumed to be constant for one nucleus. For the comparison with the experiment, Barrett equivalent radius $R_{k\alpha_B}$ defined as

$$\frac{3}{R^3_{k\alpha_B}}\int_0^{R_{k\alpha_B}} r^k e^{-\alpha_B r} r^2 \mathrm{d}r = \langle r^k e^{-\alpha_B r}\rangle \tag{4}$$

is convenient rather than the moment $\langle r^k e^{-\alpha_B r}\rangle$.

$R_{k\alpha_B}$ or $\langle r^k e^{-\alpha_B r}\rangle$ depends the index k. Because different muonic X-ray transitions correspond to different k, various pairs of $(k, R_{k\alpha_B})$ can be determined by measuring a series of muonic X-ray lines. Figure 3 illustrate $(k, R_{k\alpha_B})$ determined by the experimental data of the muonic $2p$-$1s$, $3d$-$2p$, and $4d$-$2p$ transitions of ^{108}Pd.

Similarly to the ordinary nuclear moment, a larger k corresponds to an outer distribution of the nucleus. Since larger indexes k are determined by higher transitions, this is consistent with the fact that higher X-ray transitions occur in the outer region from the nucleus.

The muonic X-ray energies can be compared with the other experiment or theory through this $(k,\ R_{k\alpha_B})$ plot, because one can calculate $R_{k\alpha_B}$ against k for arbitrary charge distribution. As shown in Fig. 3, the series of muonic transitions restrict the nuclear distribution in the (k, $R_{k\alpha_B}$) plot. Despite the higher transitions will help to further limitation, the current experimental resolution is insufficient to include the $4f$-$3d$ transition to this discussion. Furthermore, $2s$-$2p$ transition will corresponds to smaller k and inner distribution, which was not observed because of the insufficient statistics. Further progress in experimental techniques to measure $4f$-$3d$ or $2s$-$2p$ with higher resolution will drastically improve this argument.

4 Summary

The muonic X-ray energies for five palladium isotopes $^{104,105,106,108,\text{and}110}$Pd were determined experimentally by spectroscopic study in the MuSIC-M1 beamline. The nuclear charge radii for there isotopes are also deduced by assuming two parameter Fermi distribution for the nuclear charge distribution. An alternative way to restrict theoretical or experimental nuclear charge distributions by using muonic X-ray energies is proposed and demonstrated with the experimental data. In both discussions, future high resolution spectroscopic works for non-yrast transition, especially $4f$-$3d$ and $2s$-$2p$, are desired for further discussion.

References

[1] T. Y. Saito, et al., Phys. Rev. C **111**, 034313 (2025).

[2] G. Fricke et al., At. Data Nucl. Data Tables **60**, 177 (1995).

[3] I. Angeli and K. Marinova, At. Data Nucl. Data Tables **99**, 69 (2013).

[4] N. Michel, N. S. Oreshkina, and C. H. Keitel, Phys. Rev. A **96**, 032510 (2017).

[5] R. C. Barrett, Rep. Prog. Phys. **37**, 1 (1974).

[6] E. Borie and G. A. Rinker, Rev. Mod. Phys. **54**, 67 (1982).

[7] R. C. Barrett, Phys. Lett. B **33**, 388 (1970).

[8] K. W. Ford and G. A. Rinker, Phys. Rev. C **7**, 1206 (1973).

[9] I. Angeli, Acta Physica Hungaria A Heavy Ion Physics **15**, 87 (1970).

[10] S. Ebata, T. Nakatsukasa, and T. Inakura, Phys. Rev. C **90**, 024303 (2014).

[11] S. Ebata and T. Nakatsukasa Phys. Scr. **92**, 064005 (2017).

[12] J. Bartel, P. Quentin, M. Brack, C. Guet, and H.-B Hakansson, Nucl. Phys. A **386**, 79 (1982).

[13] L. B. v. d. Laan Ph.D Thesis, Amsterdam University (1986).